Investigation of a Profile Laser Scanner for its use in geodetic deformation monitoring

Victoria ROSA[1] (0009-0009-1837-1604) & Hans Neuner[2] (0000-0002-2846-1402)

[1] TU Wien, victoria.rosa@geo.tuwien.ac.at

[2] TU Wien

DOI: 10.3217/978-3-99161-070-0-020, CC BY 4.0

1 Introduction

The monitoring of large-scale infrastructures is a key issue in engineering geodesy. Terrestrial laser scanning has proven to be an effective method for such monitoring tasks. In previous works, one way to approach this task was employing a static profile laser scanner (PLS) to monitor possible displacements of an object of interest. Examples of such a setup include vibration response measurements (HESSE et al. 2006, KUTTERER et al. 2009) and bridge monitoring, particularly for slow changes (a few mm per hour) (SCHILL & EICHHORN 2019a, 2019b). Besides static use of the scanner, kinematic monitoring has become a significant research area. Mobile laser scanning systems are commonly used, for example, to monitor large-scale environments such as streets (REITERER et al., 2022) and anchored retaining structures (KALENJUK et al., 2021).

The use of cost-effective devices can potentially improve the efficiency of geodetic monitoring. Inspecting these devices beforehand is essential to assess their suitability for specific monitoring tasks. Studies on systematic effects in EO-distance measurements, such as temperature changes (GLENNIE & LICHTI 2011), long-term stability (GLENNIE et al. 2016), and the warm-up effect (RÜEGER 1996), are widespread. HEINZ et al. (2018) examined a high-end profile laser scanner and its stochastic distance characteristics at different ranges. Conversely, BAUER & WOSCHITZ (2024) conducted a comparable study with a 3D laser scanner, assessing performance over a 30 m range with a step size of 40 mm. Both studies achieved high accuracy by using a horizontal comparator bench with an interferometer as the reference.

Integrating the inspected devices into multisensor systems requires precise knowledge of their spatial offsets (lever arms) and rotational alignment (boresight angles) relative to the other sensor frames. STRÜBING & NEUMANN (2013) introduce an approach for determining the sensor frame position of four profile laser scanners on a multi-sensor platform by scanning planar surfaces. This method has been adopted, adapted and extended for applications in other studies (ERNST et al. (2022); HEINZ (2021); KHAMI et al. (2025)).

This study explores a profile laser scanner used in automation technology to evaluate its suitability for geodetic monitoring. Section 2 introduces the device, the Triple-IN PS250-90+ profile laser scanner, and reviews prior research. First, it examines the scanner's sensitivity for detecting displacements within a 30 m range, supported by reference measurements obtained

with a laser tracker. Second, it extends the correction model to account for two key device-dependent effects: transient response over days and the influence of temperature, as originally proposed by KOSTJAK & NEUNER (2023). Section 3 focuses on determining the device's sensor frame, emphasizing the impact of the four-sided rotation polygon mirror and its subsequent effects on monitoring tasks. In contrast to STRÜBING & NEUMANN (2013), the sensor frame of a single standalone device is determined directly here. The inability to measure via the zenith direction, as in ERNST et al. (2022), together with the restriction to a single circular position, poses serious challenges to finding a suitable configuration. In this work, a practically feasible approach is presented. Finally, the conclusion and outlook are presented in Section 4.

2 Test device Triple-IN PS250-90+

This section introduces the Triple-IN PS250-90+ test device. This PLS was selected for the study because it has a specified coordinate standard deviation of 5 mm, is cost-effective, and therefore has potential for geodetic monitoring applications.

2.1 Specifications

The Triple-IN PS250-90+ (serial 2921), shown in Figure 1, has dimensions of 12.1 cm x 10.9 cm x 24.7 cm (B x T x H) and weighs 2.8 kg. (TRIPLE-IN 2019). It has a robust case, making the device suitable for use in harsh conditions and operating at outdoor temperatures from -30 °C to +50 °C. Data communication and power are via Ethernet, with local network data retrieval. Distance measurements from 1.6 m can be performed with a standard deviation of 5 mm in the coordinates (up to 20 m), and up to 250 m with a standard deviation of 28 mm. The laser spot is circular at scan distances under 20 m, with a diameter of less than 5 cm. The PLS is operating in "normal mode" at a frequency of 30 Hz, using a four-sided rotation polygon mirror. Each mirror performs a sequential profile scan with 1 000 points over a 90 ° scan area (step size 0.09 °). The profile starts at 45 ° inclination from the vertical axis (see Figure 1 in the middle). The orientation of the specified coordinate system of the PLS is shown on the right of Figure 1. In monitoring applications observing slow changes at velocities of a few mm/hour, extending the measurement duration can enhance precision. Assuming uncorrelated averaged measurements over one minute, measured at 30 Hz (n_1 = 1800), with the specified standard deviation of the coordinate σ_s = 5 mm, the theoretical standard deviation of the mean is σ_{m1} = 0.1 mm (see Eq. 1), rising to σ_{m2} = 0.2 mm for single-mirror scans (n_2 = 450). The non-centrality parameter λ, corresponding to the standard deviation of the difference between two measurements σ_{diff} (Eq. 2), was calculated to identify the smallest detectable deformation. It was determined using the significance level (α = 5 %, two-sided) and the target test power (β = 20 %). The value of λ was obtained by summing the relevant quantiles of the standard normal distribution, resulting in λ_1 = 0.4 mm and λ_2 = 0.8 mm.

$$\sigma_m = \frac{\sigma_s}{\sqrt{n}} \tag{1}$$

$$\sigma_{diff} = \sqrt{2} \cdot \sigma_m \tag{2}$$

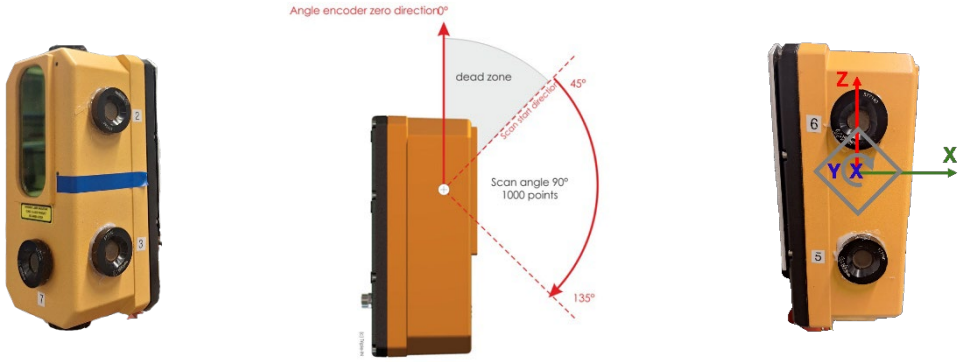

Fig. 1: Triple-IN PS250-90+ (left); Scan area (TRIPLE-IN 2019) (middle); Defined coordinate system (right);

2.2 Investigations for static measurement configurations

In KOSTJAK & NEUNER (2023), the same test device was examined for its sensitivity in detecting distance variations and its systematic effects on distance measurements. The laboratory studies discussed there are presented and expanded in this section.

Sensitivity

For the sensitivity investigation, the PLS and a laser tracker (LTD800), used as a reference, were aligned with CCR measurements at a distance of 34 m. The object, a concrete block, was moved within the line of sight of the devices. For the first 2 mm of displacement (vertical black line), the step size was 0.1-0.2 mm; thereafter, it was increased up to 4 mm to test the response to larger displacements until a total displacement of 27 mm was achieved. Displacement measurements at 4 m and 30 m from the PLS were obtained using a stop-and-go method. The schematic setup is shown in Figure 2. The PLS measured a profile over one minute along the z-axis, whereas the laser tracker monitored the movement with a corner cube reflector (CCR) mounted in a magnetic nest on the concrete block. Figure 2 (left) illustrates the deviation of the PLS measurements from the reference, plotted as a function of displacement relative to the initial measurement recorded by the laser tracker. The graphs show the mean deviation of the profile points on the object by each mirror. The histograms on the right display the distribution of differences between all measured points and the reference (red for 4 m, black for 30 m). The PLS reports the displacements equally well for both distances compared to the reference measurement. This is also reflected in the comparison of the mean values shown in the histograms, where the difference is not statistically significant. Additionally, there is no significant difference between the mirrorwise measurements. In conclusion, the PLS is able to detect small displacements (<1 mm) within a 30 m range.

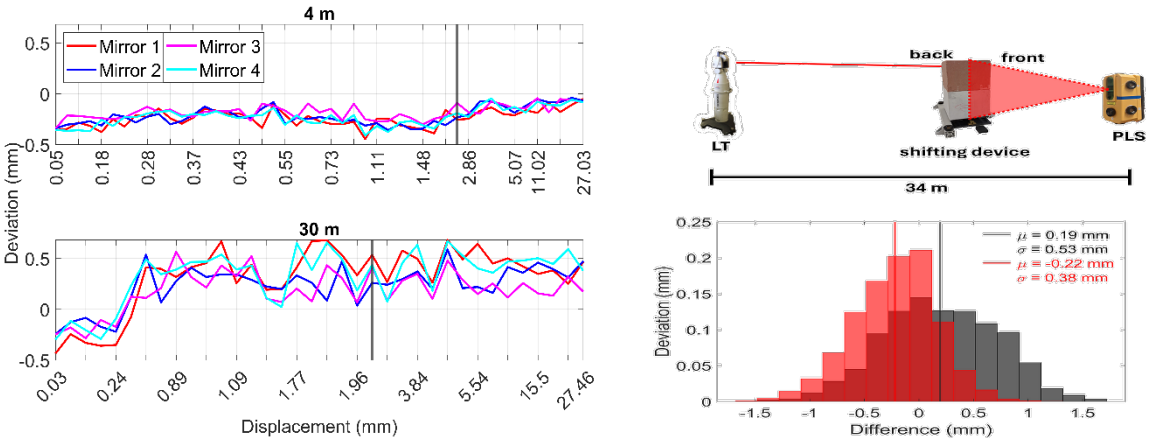

Fig. 2: Difference between PLS and reference. Mean difference of all points on the concrete block to the reference per mirror (left); histogram of differences of all points on the concrete block to the reference: red: 4 m, black: 30 m (right)

Systematic effects in the distance measurement

A correction model (Eq. 3) for investigating systematic effects in distance measurements was initially proposed by KOSTJAK & NEUNER (2023). The model consists of 3 components: correction of the exponential transient response $a\tilde{T}(1-e^{-bn})$, correction for the linear temperature dependence $c(T-\tilde{T})$, and an offset d. The behaviour of the two considered systematic effects was examined in six datasets collected over two years (2021–2023). It was found that the effects are reproducible and can be described using the same parameter set for each mirror position. In the left part of Figure 3, the top graph depicts distance variations with the median subtracted (black) at the 90° mirror position in April 2023 over a period of seven days. The measurements were taken over one minute, with a five-minute pause interval. In red, the original correction model is shown; the related parameters are listed in Table 1. In the graph on the right in Figure 3, the difference between the distance variations and the original correction model is displayed in red.

Here, the above-mentioned model is enhanced by an additional exponential term that accounts for a systematic effect identified during reanalysis of the six data sets. This effect is assumed to result from an overlying warm-up. This extension of the correction model is presented in Eq. 4 with the related parameters in Table 1. The graphs of the extended model and the difference from the distance variations are shown in Figure 3 (blue).

Both models capture the overall behaviour of the distance variation. In the original model, the transient response is described as a weak, long-term effect. The extended model splits this into a short-term effect, modelled as a warm-up (parameters g, f), and a long-term accumulation. This eliminates the long-term trend exhibited by the original model. The assumption of a short-term transient response is supported by the more accurate approximation of the course of the distance variations over the first two days. However, the long-term transient response, which lasts several days, occurs whenever the scanner is switched on. The exact cause remains unknown; therefore, a physical explanation cannot yet be included in the correction model.

$$\Delta \mathrm{D} = \left(\mathrm{D} - \widetilde{\mathrm{D}}\right) = a\tilde{T}(1 - e^{-bn}) + c\left(T - \tilde{T}\right) + d \tag{3}$$

$$\Delta \mathrm{D} = \left(D - \widetilde{D}\right) = \tilde{T}(a(1 - e^{-bn}) + g(1 - e^{-fn})) + c\left(T - \tilde{T}\right) + d \tag{4}$$

Table 1: Parameter sets for mirror position at 90 ° for both models

Parameter	Original model	Extended model
a (mm/°C)	0.049	0.035
b (mm^{-1})	$4.25 \cdot 10^{-4}$	$4.95 \cdot 10^{-4}$
c (mm/°C)	0.428	0.332
d (mm)	−1.16	−3.34
f (min^{-1})		0.029
g (mm/°C)		0.061

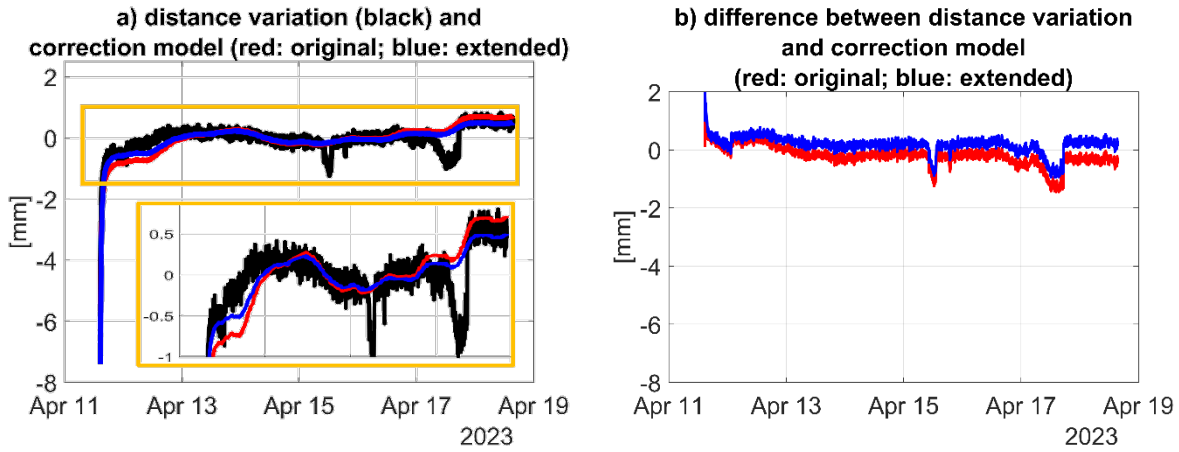

Fig. 3: Comparison of the correction models at mirror position 90 °: a) distance variation (black) and correction model (red: original; blue: extended); b) difference between distance variation and correction model (red: original; blue: extended)

3 Determination of the sensor frame

Depending on the application, two types of data collection for monitoring measurements can be distinguished. On the one hand, absolute data collection is primarily used for kinematic measurements, and on the other hand, relative data collection is used mainly for deformation analysis. In both cases, determining the sensor frame's position is important. In kinematic applications, aligning sensors with each other is crucial. It is also important to know the measurement locations on the object when performing deformation analysis. Therefore, determining the sensor frame is necessary.

As, this test device stores the profile measurements with the corresponding mirror ID, this enables an investigation of the polygon mirror and its influence on profile measurements. A sensor frame can be estimated for each mirror measurement. Alignment differences between

the single sides of the polygon can lead to different profiles being measured on the object, resulting in systematic effects.

3.1 Methodology

As noted in the introduction, a common method for determining the position of profile laser scanners uses planes. This paper presents a concept based on the approach outlined in STRÜBING & NEUMANN (2013). In this method, plates are treated as planes and scanned with two laser scanners.

In this contribution, the reference system is right-handed and realised using a laser tracker AT960 and a handheld line scanner T-Scan 5. The PLS sensor system is also right-handed, with the x-axis aligned with the scan plane (x-z plane) (see Figure 1 (right)). The approach is based on the plane equation given in Eq. (5), which states that all scanned points i lie on the same plane. The plane parameters, the normal vector $\boldsymbol{n} = [n_x, n_y, n_z]$, and the distance to the origin d, are defined in the reference system. The transformation between the two sensor frames (see Eq. (6)) can then be estimated using the plane equation condition. The point $\boldsymbol{x}_i = [x, y, z]_i$ derived from the measurements by the PLS must be part of the plane in the reference system. The rotation matrices are given in Eq. (7a-b). The estimation is performed using a Gauss-Helmert least-squares adjustment. The unknown parameters are the six transformation parameters: translation t_x, t_y, t_z and rotation r_x, r_y, r_z between the PLS sensor frame and the reference frame. The point to be transformed is introduced in the polar space as the PLS only delivers the measured distance s_d, per encoder position α.

$$\boldsymbol{n}^T \cdot \boldsymbol{x}_i - d = 0 \tag{5}$$

$$\boldsymbol{x}_i = \boldsymbol{t} + \boldsymbol{R}_x \boldsymbol{R}_y \boldsymbol{R}_z \cdot \boldsymbol{x}_i^S \text{ with } \boldsymbol{x}_i^S = \begin{bmatrix} s_d \cdot \cos\alpha \\ 0 \\ s_d \cdot \sin\alpha \end{bmatrix} \tag{6}$$

$$\boldsymbol{R}_x = \begin{bmatrix} 1 & 0 & 0 \\ 0 & \cos r_x & -\sin r_x \\ 0 & \sin r_x & \cos r_x \end{bmatrix}, \boldsymbol{R}_y = \begin{bmatrix} \cos r_y & 0 & \sin r_y \\ 0 & 1 & 0 \\ -\sin r_y & 0 & \cos r_y \end{bmatrix}, \tag{7a}$$

$$\boldsymbol{R}_x = \begin{bmatrix} \cos r_z & -\sin r_z & 0 \\ \sin r_z & \cos r_z & 0 \\ 0 & 0 & 1 \end{bmatrix} \tag{7b}$$

The plane parameters $\boldsymbol{n}$ and d, derived from the T-Scan scans, are introduced deterministically into the adjustment because of the T-Scan's high accuracy. The measured distance s_d is treated as an observation, in contrast to the encoder position α, which has deterministic values according to Eq. 8.

$$\alpha \in [0^\circ, 45^\circ] \cup (315^\circ, 0^\circ) \text{ with } \Delta\alpha = 0.09^\circ \tag{8}$$

In this contribution, in contrast to STRÜBING & NEUMANN (2013), the sensor frame of a single standalone device is determined directly through a single transformation from the PLS sensor to the reference frame. In addition, the approach presented here enables the estimation of the

sensor frame from a single device position. Due to the low opening angle of 90 ° and the minimum measuring distance of 1.6 m, the required number and arrangement of planes were adjusted accordingly. The inability to measure in two circular positions and via the zenith direction makes it challenging to find a suitable configuration. A simulation environment was developed to identify the configuration process and to understand how individual planes operate within the setup.

3.2 Laboratory setup

The PLS profile in the PLS system is shown in Figure 4 on the left. A total of 9 planes are arranged along two vertical alignments, with the planes positioned at horizontal distances of 1.8 m and 5.8 m from the test device. Figure 4 on the right shows each plane's most significant contribution (grey), identified by a decrease in correlation between parameters, to estimating the transformation parameters. This is determined by excluding that plane during the adjustment process. It is evident that several planes support a single parameter in the estimation process. In addition, the main direction of the normal vector of the plate relative to the PLS coordinate system is shown in the last column. To precisely determine the sensor frame's location, the plates must be aligned along all three coordinate axes.

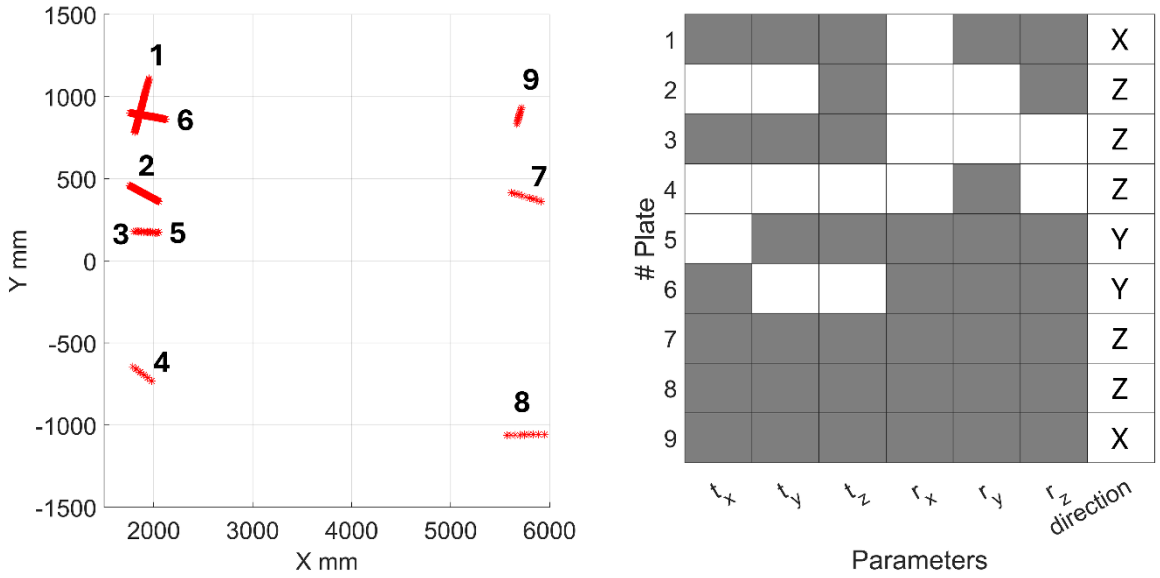

Fig. 4: Left: measured PLS profile (red). Right: Significant contribution (grey) of each plane to the estimation of the transformation parameters and main direction of the normal vector (last column).

In Figure 5, the left and middle images provide an overview of the laboratory setup. The planes are realised using white-painted aluminium plates. These are mounted on a stable frame with magnetic ball nests, which enable the establishment and fixation of each plate's orientation. The PLS is mounted on a secured tripod. The laser tracker is positioned to enable scanning of all plates with the T-Scan. Because it is not possible to scan all 9 plates simultaneously due to the need to adapt the orientation at a single position, the measurement process is divided into three sections. After setting up the plates for simultaneous scanning, the plates were first scanned

using the T-Scan (see Figure 5, right). Then, the plates were scanned using the PLS. To improve precision, one-minute scans were performed. It was ensured that the aligned plates or frame remained untouched during scanning. In addition, the measurement was performed as quickly as possible to minimise potential effects from the surroundings.

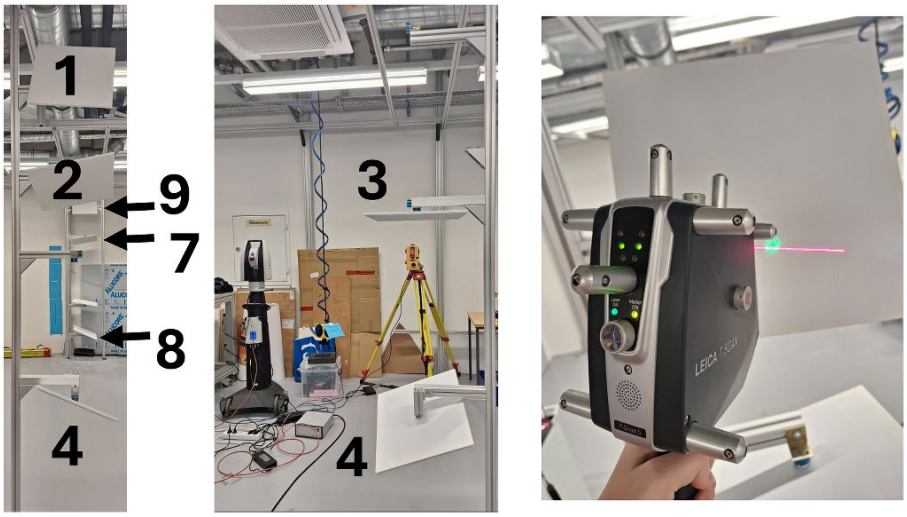

Fig. 5: Arranged plates in the laboratory, as seen from the PLS (left); Devices' positions (middle); T-Scan (right)

3.3 Results

For the evaluation, the Reference-scans taken by the T-Scan were used to estimate the plane parameters. The PLS measurements were filtered and referenced to the plane parameters. Planes scanned multiple times with both devices during the measurement process were treated separately in the least-squares adjustment. The least-squares adjustment for position estimation is performed individually for each mirror. The correlation matrix is shown in Figure 6, with the highest value of ~0.86.

Table 2 shows the estimated standard deviation of the transformation parameters for each mirror. As expected, the standard deviations are similar for the cases of the four mirrors. In the worst case, the translation parameters are determined with a standard deviation of 0.24 mm. The rotation parameters are estimated with standard deviations of max. 7.5 mgon. This is closely related to the noise level of the distance measurements introduced. The adjustment uses the scanner-provided standard deviations of the distance measurements (mean value $\bar{\sigma}_{s,prior}$). These values could be slightly lowered to pass the global test; the mean value $\bar{\sigma}_{s,post}$ is shown in Table 2. Additionally, the dimensions of the laboratory room permit only a maximum distance of 6 m. The differences between the estimated sensor frames per mirror are shown in Table 3. Bold numbers indicate values higher than the standard deviation of the difference between two mirrors. Values that exceed three times the standard deviation of the difference are shown in red.

The significant deviations in rotation about the Z-axis indicate that the profile of mirror 3 differs from those of the other mirrors. Regarding rotation about the X-axis, it can be inferred that mirrors 1 and 2 are paired, as are mirrors 3 and 4.

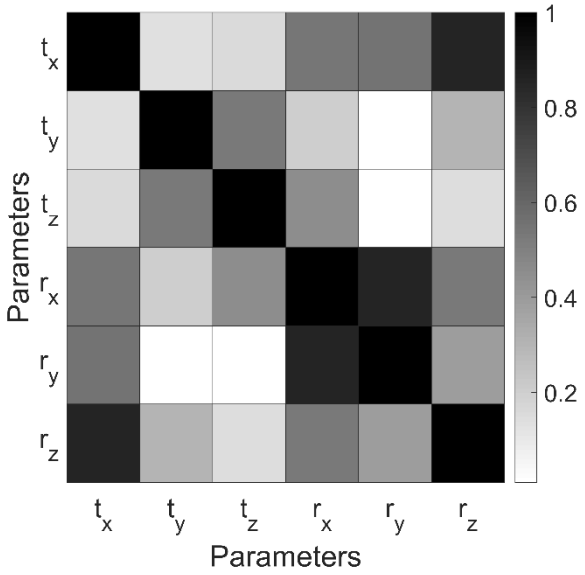

Fig. 6: Correlation matrix of the measurement

Table 2: Estimated standard deviations of the transformation parameters per mirror and mean standard deviation of the distance measurements

Mirror	σ_{t_x} (mm)	σ_{t_y} (mm)	σ_{t_z} (mm)	σ_{r_x} (mgon)	σ_{r_y} (mgon)	σ_{r_z} (mgon)	$\overline{\sigma}_{s,prior}$ (mm)	$\overline{\sigma}_{s,post}$ (mm)
1	0.20	0.13	0.10	4.0	6.6	4.8	4.3	2.6
2	0.23	0.15	0.12	4.5	7.4	5.5	4.3	2.8
3	0.24	0.15	0.12	4.6	7.5	5.6	4.3	3.0
4	0.20	0.13	0.10	3.9	6.4	4.8	4.3	2.6

Table 3: Differences between the estimated sensor frame per mirror. Bold black – values higher than the standard deviation of the difference between two mirrors; red – values that exceed three times the standard deviation of the difference between two mirrors

Mirror-difference	Δt_x (mm)	Δt_y (mm)	Δt_z (mm)	Δr_x (mgon)	Δr_y (mgon)	Δr_z (mgon)
1-2	**0.81**	**-0.33**	0.07	**-10.3**	**-11.9**	**20.0**
1-3	**1.46**	**-0.65**	**-0.31**	**38.0**	**17.2**	**44.3**
1-4	0.16	**-0.23**	-0.04	**42.7**	**19.3**	1.6
2-3	**0.64**	**-0.32**	**-0.39**	**48.3**	**29.1**	**24.3**
2-4	**-0.65**	0.10	-0.11	**53.0**	**31.2**	**-18.2**
3-4	**-1.30**	**0.42**	**0.28**	4.7	2.1	**-42.6**

The measurement results clearly show that the estimated sensor frames differ significantly in individual parameters. This demonstrates that the profile's position relative to the object yields significant differences across individual mirrors. Considering the difference between mirrors 1 and 3 of 44.3 mgon over 6 m results in a lateral deviation of 4.43 mm, whereas over 30 m it is 22.15 mm. Whether the individual origins of the sensor frames can be merged must be considered separately, depending on the application. However, the results also show that many differences exceed the calculated standard deviations, even though the threshold for significance is raised due to the high standard deviations of the estimated parameters. Reducing the estimated standard deviation could lead to more values being significant. Nonetheless, the manufacturer's specifications could be verified.

4 Conclusion and outlook

In this contribution, the Triple-IN PS250-90+ profile laser scanner was investigated for its suitability for monitoring measurements in geodesy. For this purpose, the sensitivity to deformation was tested in a laboratory experiment. The test device can detect small displacements (<1 mm) over a distance of 30 m. Additionally, an extension of the correction model, primarily proposed by KOSTJAK & NEUNER (2023), was introduced. Although it performs better than the original correction model, it cannot account for all systematic effects observed in the distance measurements. One reason is that the cause of the transient response remains unknown.

This contribution aimed to estimate the sensor frame of the investigated PLS and assess whether the sensor frames related to the four mirrors differ significantly from one another. The transformation between the mirrorwise profile scans and the reference scans was then estimated through a least-squares adjustment. The laboratory measurements show significant differences between mirror 3 and the other three mirrors in rotation about the z-axis. The maximum difference is 44.3 mgon, which corresponds to a profile spacing of 22.15 mm at a distance of 30 m. However, the standard deviation of the estimated rotation parameters between the reference system and the PLS sensor frames is several milligons. This is due to the accuracy level of the PLS.

Overall, the results indicate that the specified standard deviation of 5 mm can be confirmed. This was accomplished by scanning the same plates, considered to be planes, with the PLS and T-Scan. In the future, the correction model will be further investigated, and the laboratory setup will be refined. Improvements are planned for plate fixation and positioning. Moreover, a study will be conducted on the notable differences between mirrorwise sensor frames at higher distances, where their impact on monitoring measurements is likely to be larger.

Literature

BAUER, P. & WOSCHITZ, H. (2024): Laboratory Investigations of the Leica RTC360 Laser Scanner – Distance Measuring Performance. In: Sensors 2024, 24, 3742, https://doi.org/10.3390/s24123742.

ERNST, D., VOGEL, S., NEUMANN, I. & ALKHATIB, H. (2022): Analyse unterschiedlicher Positionskombinationen zur intrinsischen und extrinsischen Kalibrierung eines Velodyne VLP-16. In: Allgemeine Vermessungs-Nachrichten (avn) 129(2022)6, 244-252.

GLENNIE, C. L., KUSARI, A. & FACHIN, A. (2016): Calibration and Stability Analysis of the VLP-16 Laser Scanner. In: International Archives of the Photogrammetry, Remote Sensing & Spatial Information Sciences (2016)XL-3/W4, 55-60.

GLENNIE, C. L. & LICHTI, D. D. (2011): Temporal Stability of the Velodyne HDL-64E S2 Scanner for High Accuracy Scanning Applications. In: Remote Sensing 2011, 3, 539-553.

HEINZ, E. (2021): Beiträge zur Kalibrierung und Evaluierung von Multisensorsystemen für kinematisches Laserscanning. Universitäts- und Landesbibliothek Bonn.

HEINZ, E., METTENLEITER, M., KUHLMANN, H. & HOLST, C. (2018): Strategy for Determining the Stochastic Distance Characteristics of the 2D Laser Scanner Z+F Profiler 9012A with Special Focus on the Close Range. In: Sensors 2018,18,2253; doi:10.3390/s18972253.

HESSE, C., HEER, R., HORST, S. & NEUNER, H. (2006): A Concept for Monitoring Wing Energy Turbines with Geodetic Techniques – In: Kahmen, H.; Chrzanowski, A. (Eds): 3rd IAG Symposium on Geodesy for Geotechnical and Structural Engineering. 12th FIG Symposium on Deformation Measurement, Baden, Austria, (22-24 May 2006).

KALENJUK, S., LIENHART, W., REBHAN, M.J. (2021): Processing of mobile laser scanning data for large-scale deformation monitoring of anchored retaining structures along highways. In: Comput Aided Civ Inf. 2021;36:678–694. https://doi.org/10.1111/mice.12656

KHAMI, A., NEUMANN, I. & VOGEL, S. (2025): Intrinsic and extrinsic calibration of a UAV-based multi-sensor system. In: Journal of Applied Geodesy, 20(2026)1, 31-49, https://doi.org/10.1515/jag-2024-0016.

KOSTJAK, V. & NEUNER, H. (2023): Investigation of Systematic Influences on the Distance Measurement and Sensitivity of a Profile Laser Scanner. In: Allgemeine Vermessungs-Nachrichten (avn) 130(2023)4, 99-108.

KUTTERER, H., PAFFENHOLZ, J.-A., & VENNEGEERTS, H. (2009): Kinematisches terrestrisches Laserscanning. In: Zeitschrift für Geodäsie, Geoinformation und Landmanagement (zfv) 134(2009)2, 79-87.

REITERER, A., VON OLSHAUSEN, P., MAUS, P., FREY, S. SCHWARZER, S. (2022): Aufbau und Kalibration eines komplexen mobilen Multisensorsystems – Ein Überblick. In DVW e. V. – Gesellschaft für Geodäsie, Geoinformation und Landmanagement (Hrsg.), Qualitätssicherung geodätischer Mess- und Auswerteverfahren 2022 (DVW-Schriftenreihe 101, S. 53-63). Augsburg: Wißner-Verlag.

RÜEGER, J. M. (1996): Electronic Distance Measurement: An Introduction (4th ed.). Springer. ISBN 978-3-540-61159-2.

SCHILL, F. & EICHHORN, A. (2019A): Profilscanning bei Belastungsversuchen an einer Mauerwerksbrücke. In: Hanke. K; Weinold, T. (Eds.) 20. Internationale Geodätische Woche Obergurgl 2019. Wichmann, Berlin/Offenbach.

SCHILL, F. & EICHHORN, A. (2019B): Deformation Monitoring of Railway Bridges with a Profile Laser Scanner. In: Zeitschrift für Geodäsie, Geoinformation und Landmanagement (zfv) 144(2019)2, 109-118.

STRÜBING, T. & NEUMANN, I. (2013): Positions- und Orientierungsschätzung von LIDAR-Sensoren auf Multisensorplattformen. In: Zeitschrift für Geodäsie, Geoinformation und Landmanagement (zfv) 138(2013)3, 210-221.

TRIPLE-IN GMBH (2019): PSxxx-90_UserManual.pdf – Triple-IN GmbH 2019/03/06 User Manual PSxxx-90+ Laser Scanners.